Featuring work from the Single Molecule Biophysics Laboratory of Hermann E. Gaub, Center for Nano-Science, Ludwig-Maximilians-Universität München, Germany.

Title: Protein–DNA force assay in a microfluidic format

Protein–DNA interaction forces are studied using a miniaturized and multiplexed molecular force assay on a microfluidic MITOMI chip and with a new confocal analysis method.

PAPER

Protein–DNA force assay in a microfluidic format†

Marcus Otten, Philip Wolf and Hermann E. Gaub

The detailed study of protein–DNA interactions is a core effort to elucidate physiological processes, including gene regulation, DNA repair and the immune response. The molecular force assay (MFA) is an established method to study DNA-binding proteins. In particular, high-affinity binder dissociation is made possible by the application of force. Microfluidic lab-on-a-chip approaches have proven helpful for parallelization, small sample volumes, reproducibility, and low cost. We report the successful combination of these two principles, forming a microfluidic molecular force assay and representing a novel use for the established MITOMI chip design. We present, characterize, validate and apply this integrated method. An alternative confocal fluorescence microscopy readout and analysis method is introduced and validated. In a multiplexing application, EcoRI binding is detected and characterized. This method paves the way for quantitative on-chip force measurements. It is suited for integration with DNA micro-spotting and *in vitro* expression of transcription factors to form a high-throughput chip for detailed DNA–protein interaction studies.

Introduction

DNA–protein studies

Interactions between proteins and DNA are ubiquitous in living systems. Most prominently, DNA-binding transcription factors regulate gene expression.[1] Furthermore, proteins are involved in DNA repair[2,3] and the immune response.[4] In each of these tasks, the binding process and forces involved are crucial for function and can only be understood by combining a range of measurements, including affinity,[5] specificity,[6,7] turnover[8] and binding force.[9] As a most prominent example, transcription factor binding and turnover dynamics are a better predictor for functional regulation than mere occupancy levels.[10] A variety of methods for measuring DNA–protein interactions have been proposed, which differ most notably in measurement environment (*in vivo versus in vitro*), in washing requirements, in labeling needs, and in multiplexing capabilities. Chromatin-immunoprecipitation (ChIP)-based methods[11] have proven very valuable for *in vivo* measurements, despite the need for specialized antibodies for precipitation. Protein-binding microarrays (PBM)[12,13] are well suited to detect high affinity binding sequences for a given protein, if available in high amounts. Yeast-one-hybrid (Y1H)[14,15] and bacterial one-hybrid (B1H)[16] approaches are typically used to determine the proteins that bind to a given DNA sequence and are thus complementary to ChIP and PBM. High-throughput versions have been proposed.[17] These methods have a common set of drawbacks, including the need for labeling antibodies, low sensitivity or resolution and lack of parallel screening of multiple DNA sequences against multiple proteins and multiple references. This highlights the need for integrated methods, which will help overcome these drawbacks.

The molecular force assay

The molecular force assay (MFA) is an established method to probe intermolecular bonds, *e.g.* DNA–protein interactions. A probe bond and a known reference are assembled in series on a surface, bond-breaking forces are applied *via* surface retraction and a fluorescence readout reveals the bond rupture site. This approach has numerous advantages, including high sensitivity, statistical significance, its ability to detect both weak and strong binders and its independence of binder labels. Its sensitivity is due to the use of single molecules as the reference force sensor. Statistics are readily assembled in a single run, because many bonds are probed in parallel on a surface. By tuning the reference bond *via* its length, one can adapt to binders of varying strength. The active force load upon surface retraction speeds up unbinding of strong binders, up to dissociation constants in the pM range. The force probe DNA oligomers are labeled and used for the fluorescent readout, but these fluorophores are not directly at the probe or binding sites. The binder is not labeled. MFA has been used for a variety of applications and alterations of the DNA, including mismatches,[18] methylation[19] or hydroxymethylation[20] have been shown to be detectable. Its measurement principle has been applied to the binding of transcription factors, nucleases and polyamides[21] and RNA–protein interactions.[22]

Lehrstuhl für Angewandte Physik and Center for Nanoscience (CeNS), Ludwig-Maximilians-Universität, Amalienstrasse 54, 80799 Munich, Germany

Microfluidics and MITOMI

The advent of microfluidics and lab-on-a-chip technologies has recently spurred miniaturization and parallelization of tried-and-tested methods. Advantages include smaller sample volumes, higher throughput, facilitated reproducibility and reduced experimental time. One particular variant of microfluidics involves the use of multi-layer soft lithography, as pioneered by Quake *et al.*[23] One layer, the flow layer, can be used for biochemical reactions, whereas another is used to control these flows by application of pneumatic pressure. With respect to the study of protein–DNA interactions, Maerkl and Quake applied these design principles to obtain what is now known as the MITOMI chip, acronym for mechanically induced trapping of molecular interactions.[24] A button valve is used to seal and protect the sample area from contamination by neighbors or from stringent washing.[25] The chip has been applied to measure a variety of other interactions, including protein–protein[26] and protein–RNA.[27] In some cases, reaction chambers have been used for *in vitro* expression of the proteins to be probed.[26] Recently, the chip design

has been improved for fast response times and the chip is now capable of recording association and dissociation traces.[28]

In the present publication, we introduce a novel method, which for the first time combines the MFA measurement principle with a microfluidic design. In particular, the button valve of the MITOMI chip is used to apply the force necessary for bond rupture. We characterize the setup, validate it by comparison to non-microfluidic measurements, introduce a novel readout and analysis route and apply it to detect a model binder, the endonuclease EcoRI, which shows no nuclease activity in the absence of its cofactor Mg^{2+}.

Results & discussion

Method summary

The microfluidic chip design is identical to the 640-chamber MITOMI chip introduced by Maerkl and Quake.[24] The chips are produced by two-layer soft lithography of polydimethylsiloxane (PDMS). The inner walls of the flow layer display covalently attached DNA duplexes after a series of treatments
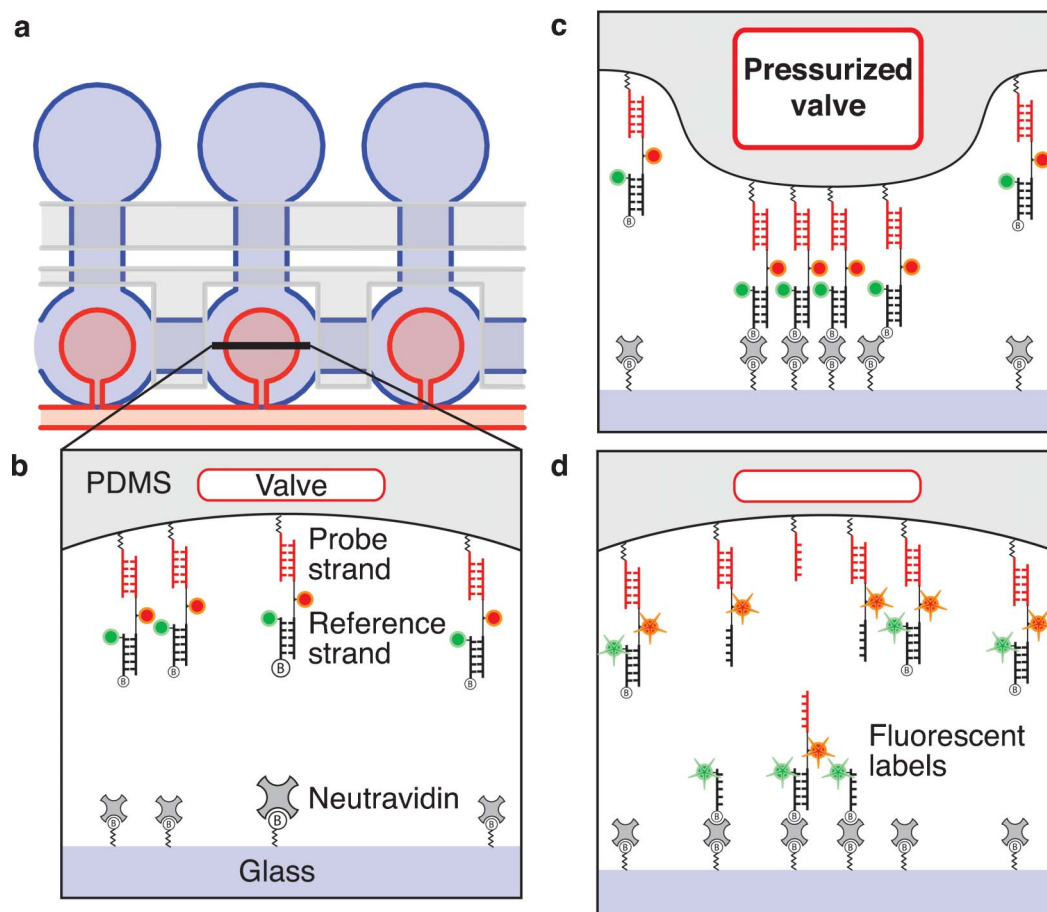

Fig. 1 Experimental design. (a) shows three of 640 double chambers in the flow layer (blue) and the overlying control layer valves (red and grey), which can expand into the flow layer by pneumatic pressure. (b) shows the initial distribution of PEG–biotin–neutravidin complexes at the glass surface and PEG–DNA probe–fluorophore–biotin complexes along the flow layer PDMS wall. (c) Actuation of the button valve establishes contact between the glass and PDMS surfaces within the button valve region only. (d) After pressure release and button retraction, the fluorophore distribution is recorded on a confocal fluorescence readout. Transferred Cy3 fluorophores (green) denote the coupling efficiency, whereas transferred Cy5 (red) is a measure of the force probes broken at the top DNA duplex bond.
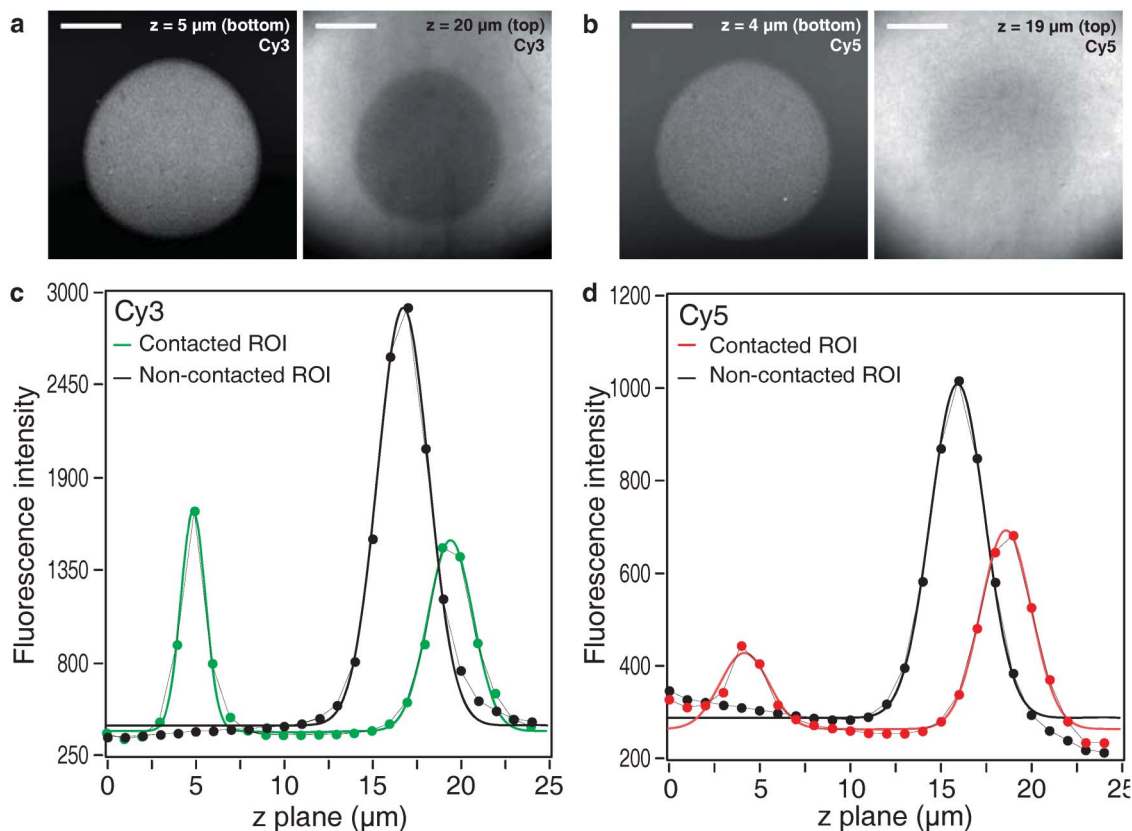
Fig. 2 Single-chamber data readout. (a) and (b) show fluorescence images of the Cy3 and Cy5 channels, respectively. The bottom glass surface slices and top PDMS surface slices are shown after button retraction. The bottom slices show transferred fluorophores and DNA strands, which are missing from the top surfaces. Scale bar: 25 μm. (c) and (d) show the vertical intensity profiles of the Cy3 and Cy5 channels, respectively. The mean intensity of the two regions of interest (ROI) is computed and plotted (dots) against the z slice position and fitted with Gaussian functions (lines). The contacted ROI (under the button valve) data is shown in color (green or red), the non-contacted ROI (to the side of the chamber) is shown in black. The Gaussian fit data serve for all follow-up analysis. The vertical shifts between the contacted and non-contacted ROI data are due to the PDMS chamber curvature.

with hydrochloric acid, aminosilane, NHS–polyethylene glycol–maleimide, and thiolized DNA oligomers[29,30] (Supplemental Fig. 1, ESI†). After bonding the functionalized chip to a neutravidin-coated glass slide, the button valve of the PDMS control layer is actuated by a linear pressure increase. Upon button retraction, one of the bonds will give, according to their relative rupture probabilities. The relative fluorophore distributions (top vs. bottom surfaces, or contacted vs. non-contacted regions) are determined by confocal fluorescent microscopy and analyzed to determine the relative rupture probabilities of the DNA duplex bonds (Fig. 1). The Cy3 transfer is proportional to the coupling efficiency of the biotin–neutravidin bond, whereas the location of the Cy5 signal reveals the stronger bond. For a more detailed description of the experimental workflow, we refer to the ESI†.

MFA principle & characterization

Fig. 1 shows the experimental design and measurement principle of the MFA. Each of the 640 chambers of the MITOMI chip displays two DNA duplexes in series at the top PDMS surface. The known bond will serve as a reference whereas the other one is the probe. By actuation of the button valve, a circular region is brought into contact with the glass

surface underneath and coupling occurs via biotin–neutravidin interactions. Upon pressure release and button retraction, both duplexes are probed under force and one of them ruptures,[31] with probabilities related to their relative strengths.[31] The fluorophores attached to strands 2 and 3 allow for their localization by confocal fluorescence imaging.

We characterize the button valve actuation by reflection interference contrast microscopy. The spatial succession of the interference maxima and minima reveals the shape of the PDMS button just prior to glass contact. We find the surface to be parabola-shaped with high reproducibility. The temporal succession of the interference maxima and minima reveals the approach and retraction velocities of this surface perpendicular to the glass surface. The approach and retraction speed can be controlled by variation of the pressure slope. In the present publication, this slope was chosen to be 0.1 psi s^{-1}, ensuring an equal valve actuation across all chambers and chips. We find good agreement between the approach velocity of 0.23 μm s^{-1}, and the retraction velocity of 0.26 μm s^{-1}, independent of the radial distance from the parabola tip (Supplemental Fig. 2, ESI†). These values are compatible with the low speeds of the piezoelectric actuator used in previous MFA implementations between 0.2 and 20 μm s^{-1}.
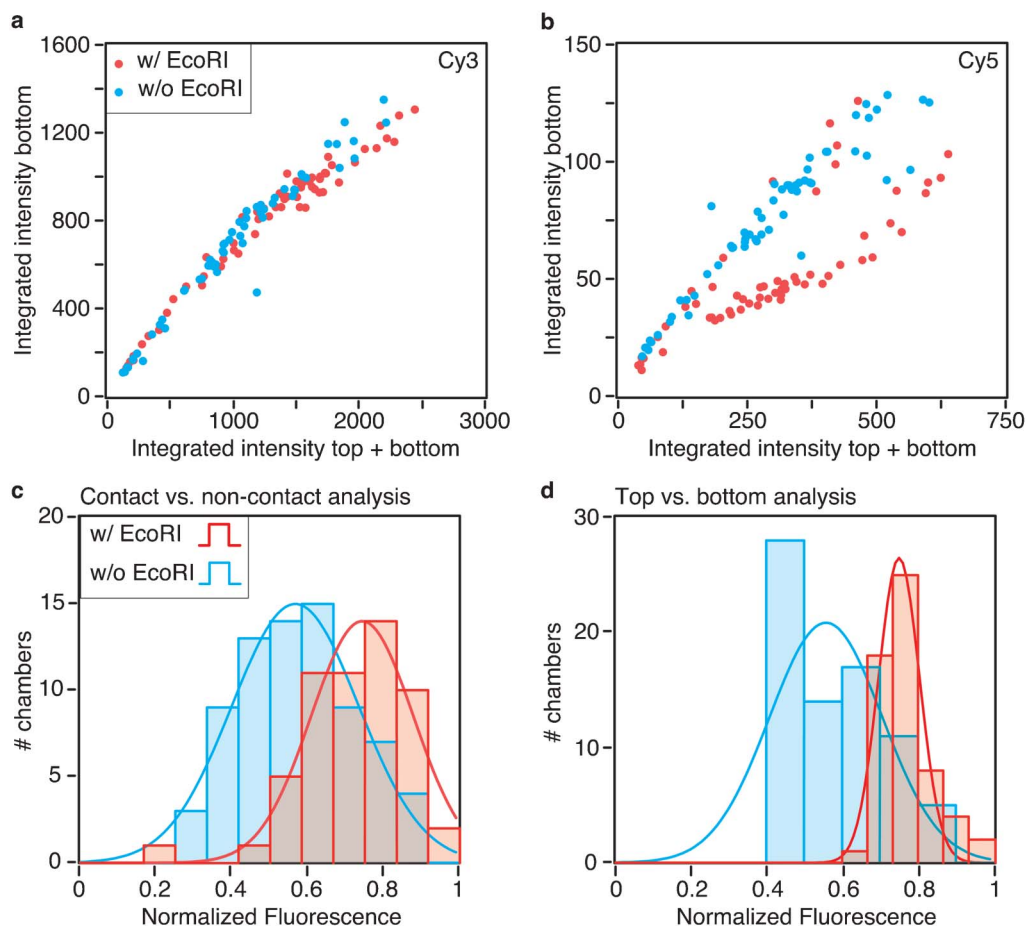
Fig. 3 Chip analysis. (a) and (b) show scatter plots of Cy3 and Cy5 intensity data from hundreds of chambers, respectively. For each chamber the integrated bottom signal is plotted against the sum of its integrated bottom and top signals in the contacted ROI only. (c) and (d) show histograms of the normalized fluorescence (corresponding to the relative bond rupture probability) computed using the contact-*vs.*-non-contact and top-*vs.*-bottom analysis methods, respectively. The histograms are fitted with Gaussian distributions. The histograms and fits are shown with and without the presence of EcoRI binders (red and blue, respectively).

Multiple key differences to previous MFA implementations emerge. First, the force application occurs by pneumatic means, rather than by a voltage-controlled piezo element. No bulk PDMS can dampen the retraction movement, which allows more direct control of the retraction speed. Second, the contact and separation occurs between a flat glass surface and a rounded PDMS surface, as opposed to two planar surfaces. This is predicted to be a more favorable geometry to avoid non-linear retraction effects. Soft lithography and photoresist reflow are versatile tools to tune the actuation of this membrane.[32] Third, the small distance separating the two fluorescent surfaces facilitates comparable readouts of both surfaces. Previously, only the glass surface was analyzed. This additional set of data opens up a top-*vs.*-bottom analysis route, rather than the traditional contact-*vs.*-non-contact method.

Comparison of analysis methods

The data readout and analysis for a single chamber are shown in Fig. 2. Confocal scans are performed identically for two fluorescent channels, Cy3 and Cy5. The Cy5 signal is a measure of the number of transferred middle strands, whereas the Cy3 signal is a measure of the coupling efficiency of the probe *via* biotin–neutravidin bonding to the glass surface. The contacted region of interest (ROI) beneath the button valve shows fluorescence signals both at the glass surface and at the PDMS surface, whereas the non-contacted ROI shows no fluorescence transfer from the PDMS onto the glass surface, as can be seen in Fig. 2c and 2d. Both distributions can be fitted with Gaussian functions. This data collection opens up two alternative analysis routes: (1) a contact-*vs.*-non-contact method similar to the previously introduced MFA analysis, and (2) a top-*vs.*-bottom method. The first compares the two regions at the PDMS surface to determine the missing dye fraction at the contacted ROI, whereas the second method compares the two peaks of the contacted ROI to determine the transferred dye fraction.

The quantity of interest is the relative rupture probability of the two bonds. On the basis of previous MFA studies, it is named "normalized fluorescence" (NF) and denotes the fraction of probes ruptured at the lower bond, normalized to the number of probes coupled and under load. It is thus equivalent to the relative rupture probability of the two bonds. It can be expressed as follows for the contact-*vs.*-non-contact
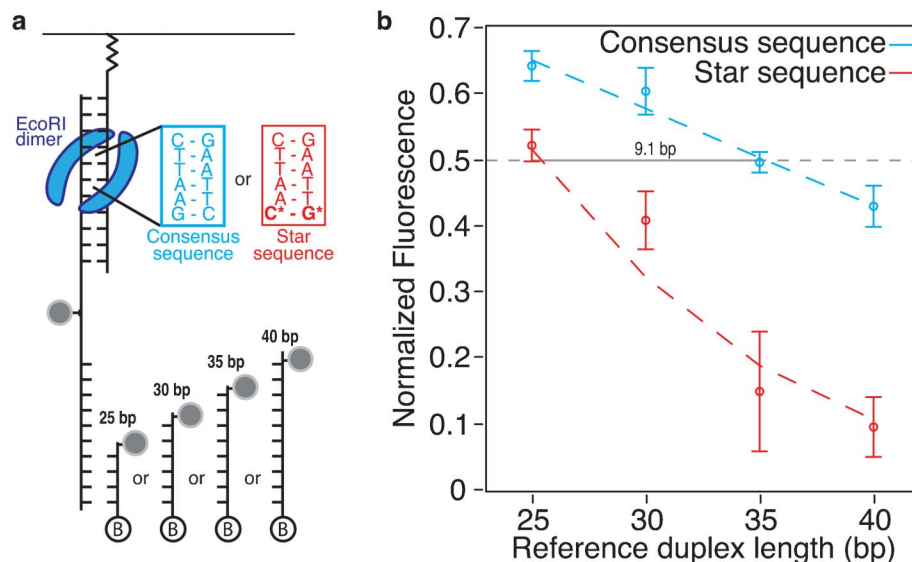
Fig. 4 Multiplexing application. (a) shows the multiplexed design of DNA strands to form molecular force probes displaying either the EcoRI consensus sequence GAATTC (blue) or the star sequence GAATTG (red) and to be probed against references of varying lengths (25–40 bp). Each construct is flushed into a separate microfluidic row on the same chip. (b) shows the dependence of the median normalized fluorescence in the case where EcoRI is presented to the probes shown in (a). The drop in NF upon sequence variation (from consensus to star) and upon reference elongation characterizes the specific binding and mechanical stabilization by EcoRI. The experimental results (circles, error bars) can be fitted with a Bell–Evans model simulation (dashed lines) with very good agreement.

analysis:

$$NF = \frac{\dfrac{Cy5_t^c}{Cy5_t^{nc}} - \dfrac{Cy3_t^c}{Cy3_t^{nc}}}{1 - \dfrac{Cy3_t^c}{Cy3_t^{nc}}}$$

and for the top-*vs.*-bottom method:

$$NF = 1 - \frac{\dfrac{Cy5_b^c}{Cy5_t^c + Cy5_b^c}}{\dfrac{Cy3_b^c}{Cy3_t^c + Cy3_b^c}}$$

with the following notation: $channel_{location}^{region}$, where channel is either Cy3 or Cy5, region is either c (contacted) or nc (non-contacted), and location is either t (top) or b (bottom). All intensity values are computed by integration of the respective Gaussian fit curves (background excluded). The two analysis routes are evaluated for consistency. Considering bare DNA probes in the absence of binders, we obtain a median normalized fluorescence of 0.56 ± 0.03 (s.d.) for the contact-*vs.*-non-contact analysis and of 0.55 ± 0.03 for the top-*vs.*-bottom method. The slight deviation from the symmetric distribution can be attributed to different polyethylene glycol linker lengths at the glass and PDMS surfaces. Furthermore, the fluorescence dyes are expected to show excitation and emission characteristics dependant on the local environment, which differ at the glass and the PDMS surfaces.[33] This very good agreement underlines the equivalence of the two analysis methods. The top-*vs.*-bottom analysis route is possibly less prone to errors. Uneven illumination, inhomogeneous surface functionalization and optical effects are excluded as possible sources of error. Previously, these were corrected for by taking an additional set of images at the beginning of the experiment. In particular for

high-throughput implementations, this leads to a longer experiment time and to fluorophore bleaching.

EcoRI detection

An exemplary demonstration of the DNA–protein binding detection by MFA is the effect of EcoRI binding, in the absence of its nuclease cofactor. The top DNA duplex contains the palindromic consensus sequence 5′-GAATTC-3′. Upon binding, we expect the consensus sequence to be strengthened and the rupture probabilities to shift towards the non-binding reference duplex. Fig. 3 shows the effect of EcoRI binding for a single, representative chip with statistics from 140 chambers. While the coupling efficiency, determined by the fraction of transferred Cy3 fluorophores, is not affected (Fig. 3a), the transfer of Cy5-containing middle strands is reduced in the presence of EcoRI (Fig. 3b). These differences in transfer translate into shifted distributions of normalized fluorescence values. For the contact-*vs.*-non-contact analysis method, the median of the chambers shifts from 0.56 to 0.73 (Fig. 3c). For the top-*vs.*-bottom analysis method, it shifts from 0.54 to 0.75 (Fig. 3d). These values are in good agreement with each other. Literature values from previous MFA studies with 20 bp oligomer samples and references show the same trend, with slightly differing absolute values, namely an increase from 0.48 to 0.62.[21] However, these differences may be explained by the oligomers' differences in length and in G/C content.

Multiplexing

The row-by-row multiplexing capabilities of the present experimental design are assessed by measuring EcoRI binding onto two different binding sequences (the EcoRI consensus sequence 5′-GAATTC-3′, and the star sequence 5′-GAATTG-3′) against four reference strands of varying lengths between 25

and 40 base pairs, on the same chip. Statistical significance for all 8 combinations is aimed for by preparing multiple chambers with the same combination of probe and reference. The variation of the normalized fluorescence dependent on the reference duplex length and the binding sequence composition is shown in Fig. 4. A drop in NF for increasing reference duplex length is indicative of a decreasing fraction of probes rupturing at the reference duplex. This observation is consistent with expectations and previous studies.[21] At the same time, the consensus sequence probe shows consistently higher NF values at all reference lengths, which indicates a more stable top duplex, in accordance with the expected higher binding affinity.[34,35] The data shown in Fig. 4 facilitates the quantitative understanding of the difference in EcoRI binding between its consensus and star sequences. At an equilibrated rupture probability of NF = 0.5, the mechanical stabilizing action of EcoRI binding to its consensus sequence is equivalent to an addition of 9.1 bp dsDNA in the reference strand. This analysis is supported by the very good agreement of the experimental results with a fit based on the Bell–Evans model.[36]

Conclusion

In the present publication, we have introduced a versatile method for the quantification of DNA–protein interactions, based on the application of pneumatic forces in a microfluidic chip. Upon force load, the relative rupture probabilities of two molecular bonds in series are determined by confocal fluorescence readout. We have characterized the method, with respect to the geometry and dynamics of the button valve. The method was validated with a known all-DNA probe. Then, we have introduced and validated an alternative analysis route, based on the comparison of the fluorophore distributions at the top and bottom surfaces of the sample chamber. Finally, we have applied the method to the study of EcoRI binding. This application involving multiple target and reference strands has illustrated the multiplexing capabilities of the setup. EcoRI was used as a model protein in this proof-of-principle experiment. It can readily be substituted, thus paving the way for studies of currently unknown protein–DNA interactions, including those of transcription factors. In particular, the binding forces of transcription factors were found to correlate strongly with functional regulation, more strongly even than occupancy levels.[10] Therefore, it is very promising to use the presented method with various protein variants and/or binding sequences. The multiplexing capabilities of the setup can be further expanded. DNA array microspotting technology has been shown to be compatible with the MFA without loss of validity.[21] One can choose to spot different binding and/or reference sequences. The chip also features back chambers for the spotting of cDNA plasmids or PCR products and for the expression of DNA binding protein. This on-chip expression will further increase multiplexing.

References

1 A. Ozdemir and A. Stathopoulos, *Nat. Methods*, 2011, **8**, 1016–1017.
2 J. Jiricny, *Nat. Rev. Mol. Cell Biol.*, 2006, **7**, 335–346.
3 S. P. Jackson and J. Bartek, *Nature*, 2009, **461**, 1071–1078.
4 V. Hornung and E. Latz, *Nat. Rev. Immunol.*, 2010, **10**, 123–130.
5 R. Nutiu, R. Friedman, S. Luo, I. Khrebtukova, D. Silva, R. Li, L. Zhang, G. Schroth and C. Burge, *Nat. Biotechnol.*, 2011, **29**, 659–664.
6 G. D. Stormo and Y. Zhao, *Nat. Rev. Genet.*, 2010, **11**, 751–760.
7 M. T. Weirauch, A. Cote, R. Norel, M. Annala, Y. Zhao, T. R. Riley, J. Saez-Rodriguez, T. Cokelaer, A. Vedenko, S. Talukder, D. Consortium, H. J. Bussemaker, Q. D. Morris, M. L. Bulyk, G. Stolovitzky and T. R. Hughes, *Nat. Biotechnol.*, 2013, **31**, 126–134.
8 T. S. Karpova, M. J. Kim, C. Spriet, K. Nalley, T. J. Stasevich, Z. Kherrouche, L. Heliot and J. G. Mcnally, *Science*, 2008, **319**, 466–469.
9 J. L. Arlett, E. B. Myers and M. L. Roukes, *Nat. Nanotechnol.*, 2011, **6**, 203–215.
10 C. R. Lickwar, F. Mueller, S. E. Hanlon, J. G. Mcnally and J. D. Lieb, *Nature*, 2012, **484**, 251–255.
11 C. E. Massie and I. G. Mills, *EMBO Rep.*, 2008, **9**, 337–343.
12 M. L. Bulyk, X. Huang, Y. Choo and G. M. Church, *Proc. Natl. Acad. Sci. USA*, 2001, **98**, 7158–7163.
13 G. Badis, M. F. Berger, A. A. Philippakis, S. Talukder, A. R. Gehrke, S. A. Jaeger, E. T. Chan, G. Metzler, A. Vedenko, X. Chen, H. Kuznetsov, C.-F. Wang, D. Coburn, D. E. Newburger, Q. Morris, T. R. Hughes and M. L. Bulyk, *Science*, 2009, **324**, 1720–1723.
14 H. Yokoe and R. R. Anholt, *Proc. Natl. Acad. Sci. USA*, 1993, **90**, 4655–4659.
15 J. J. Li and I. Herskowitz, *Science*, 1993, **262**, 1870–1874.
16 X. Meng, M. H. Brodsky and S. A. Wolfe, *Nat. Biotechnol.*, 2005, **23**, 988–994.
17 K. Hens, J.-D. Feuz, A. Isakova, A. Iagovitina, A. Massouras, J. Bryois, P. Callaerts, S. E. Celniker and B. Deplancke, *Nat. Methods*, 2011, **8**, 1065–1070.
18 C. Albrecht, K. Blank, M. Lalic-Mülthaler, S. Hirler, T. Mai, I. Gilbert, S. Schiffmann, T. Bayer, H. Clausen-Schaumann and H. E. Gaub, *Science*, 2003, **301**, 367–370.
19 P. M. D. Severin, X. Zou, H. E. Gaub and K. Schulten, *Nucleic Acids Res.*, 2011, **39**, 8740–8751.
20 P. M. D. Severin, X. Zou, K. Schulten and H. E. Gaub, *Biophys. J.*, 2013, **104**, 208–215.
21 P. M. D. Severin and H. E. Gaub, *Small*, 2012, **8**, 3269–3273.
22 K. Limmer, D. Aschenbrenner and H. Gaub, *Nucleic Acids Res.*, 2013, **41**, e69.

23 M. Unger, H.-P. Chou, T. Thorsen, A. Scherer and S. R. Quake, *Science*, 2000, **288**, 113–116.

24 S. J. Maerkl and S. R. Quake, *Science*, 2007, **315**, 233–237.

25 J. L. Garcia-Cordero and S. J. Maerkl, *Chem. Commun.*, 2013, **49**, 1264–1266.

26 D. Gerber, S. J. Maerkl and S. R. Quake, *Nat. Methods*, 2009, **6**, 71–74.

27 L. Martin, M. Meier, S. M. Lyons, R. V. Sit, W. F. Marzluff, S. R. Quake and H. Y. Chang, *Nat. Methods*, 2012, **9**, 1192–1194.

28 M. Geertz, D. Shore and S. Maerkl, *Proc. Natl. Acad. Sci. USA*, 2012, **109**, 16540–16545.

29 N. R. Glass, R. Tjeung, P. P. Y. Chan, L. Y. Yeo and J. R. Friend, *Biomicrofluidics*, 2011, **5**, 036501.

30 J. L. Zimmermann, T. Nicolaus, G. Neuert and K. Blank, *Nat. Protoc.*, 2010, **5**, 975–985.

31 G. Neuert, C. H. Albrecht and H. E. Gaub, *Biophys. J.*, 2007, **93**, 1215–1223.

32 P. M. Fordyce, C. A. Diaz-Botia, J. L. DeRisi and R. Gomez-Sjoberg, *Lab Chip*, 2012, **12**, 4287–4295.

33 M. Levitus and S. Ranjit, *Q. Rev. Biophys.*, 2011, **44**, 123–151.

34 D. R. Lesser, M. R. Kurpiewski and L. Jen-Jacobson, *Science*, 1990, **250**, 776–786.

35 N. Y. Sidorova and D. C. Rau, *Biophys. J.*, 2004, **87**, 2564–2576.

36 E. Evans and K. Ritchie, *Biophys. J.*, 1999, **76**, 2439–2447.